Journal of Fluorescence, Vol. 5, No. 4, 1995

Myosin Head Rotation in Muscle Fibers Measured Using Polarized Fluorescence Photobleaching Recovery

Edward H. Hellen,[1,2] Katalin Ajtai,[1] and Thomas P. Burghardt[1,3]

Received October 25, 1994; revised March 16, 1995; accepted March 17, 1995

The technique of polarized fluorescence photobleaching recovery (PFPR) has been applied for the first time to investigation of the rotational correlation time of the myosin head in muscle fibers. This is a novel application of PFPR because it is the first time PFPR has been applied to a sample which is not cylindrically symmetric about the optical axis. Therefore we present a method for analysis of PFPR results from an oriented sample such as the muscle fibers aligned perpendicularly to the optical axis used here. Control experiments performed on fluorescently labeled myosin heads in solution demonstrate that, under some conditions, our PFPR apparatus can easily measure a rotational correlation time of less than 200 μs. Validity of this application of PFPR to muscle fibers is provided by the agreement of our results with published results from a variety of other spectroscopic techniques. In particular, using glycerinated rabbit psoas muscle fibers, we find that for relaxed fibers and isometrically contracting fibers, the myosin heads undergo high-amplitude rotations on the submillisecond time domain. For fibers in rigor the myosin heads are highly oriented and nearly immobile. For fibers in ADP the myosin heads are highly ordered in a distribution quite different from that in rigor, and they are slightly more mobile than in rigor.

KEY WORDS: Muscle contraction; cross-bridge rotation; polarized fluorescence photobleaching recovery.

INTRODUCTION

The molecular mechanism of muscle contraction involves the relative movement of myosin and actin filaments driven by the hydrolysis of ATP in the myosin head or cross-bridge. It is widely accepted that the cross-bridge, or a large part of it, undergoes a rotation while attached to actin to impel one filament relative to the other and that the impulsive force is from transduction of chemical energy liberated in ATP hydrolysis. For some time now we have used spectroscopic probes to investigate the steady-state orientation of specific sites on the cross-bridge and we have determined the path and extent of cross-bridge rotation in the course of its activated cycle.[1–4] In this work we introduce for the first time the application of the time-resolved technique of polarized fluorescence photobleaching recovery (PFPR) to the investigation of the rotational dynamics of the cross-bridge. Our goal is to characterize the time scale and range of cross-bridge rotation in four physiological states of the muscle fiber including isometric contraction.

Rotation of the myosin head in muscle fibers has been investigated on the submillisecond time scale with EPR[5–7] and phosphorescence.[8,9] These methods are limited to submillisecond investigations due to the fixed lifetimes of the signals generated from the probes. PFPR does not depend on the fluorescence lifetime and therefore can investigate arbitrarily long time scales. PFPR has been used to detect rotation on the time scale of microseconds[10] to minutes.[11] A previous investigation

[1] Department of Biochemistry and Molecular Biology, Mayo Foundation, Rochester, Minnesota 55905. e-mail: burghardt@mayo.edu.
[2] Present address: Department of Physics and Astronomy, University North Carolina–Greensboro, Greensboro, North Carolina 27412.
[3] To whom correspondence should be addressed.

1053-0509/95/1200-0355$07.50/0

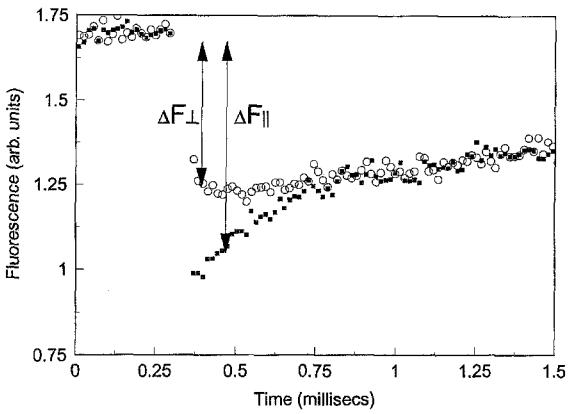

Fig. 1. Polarized fluorescence photobleaching recovery curves for 5'-IATR-labeled S1 in 70% glycerol at $T = -30°C$. The photobleaching pulse was 5 μs in duration and occurred at $t = 0.3$ ms. The bleach polarization was parallel to the illumination polarization for the filled squares and perpendicular for the open circles.

on the millisecond time scale used fluctuations of polarized fluorescence to measure myosin head rotation in fibers.[12]

This study is the first application of PFPR to myosin head rotation in muscle fibers. Therefore control experiments were performed on samples of the rhodamine-labeled myosin head, R-S1, tumbling in solution which demonstrate that, under some conditions, our PFPR apparatus can easily measure rotational correlation times for the myosin head of less than 200 μs. Additional control experiments were performed on rhodamine B immobilized in silicone vacuum grease.

This is also the first time that PFPR has been applied to a sample which is not either completely isotropic or cylindrically symmetric about the optical axis. Therefore we present a method for analysis of PFPR results obtained from an oriented sample such as the muscle fibers aligned perpendicularly to the optical axis as used here. This analysis required knowledge of the orientational distribution of the dipoles of the rhodamine labeling the myosin in muscle fibers. Orientational distributions of EPR probes[2,3,13–15] and fluorescent probes[4,16–21] labeling myosin have been investigated previously. Simultaneous multiprobe analysis combining EPR and fluorescent probe data has recently been developed and applied to muscle fibers.[1,22] Here we use steady-state fluorescence polarization measurements to determine a simple model of the orientational distribution.

In spite of some problems which arose and are discussed, the success of this initial application of PFPR to muscle fibers is demonstrated by the general agreement of our results with the previously mentioned published results from other spectroscopic techniques. In particular, we find that the range of rotation of myosin heads in glycerinated muscle fibers is nearly immobile in rigor, slightly more mobile in ADP, nearly free in relax, and between ADP and relax for active isometric contraction. In all cases the dominant rotations were faster than the millisecond time scale which was investigated for the fibers.

THEORY

PFPR of Oriented Samples

The time-resolved anisotropy produced in polarized fluorescence photobleaching recovery (PFPR) experiments has been successfully used to measure rotational correlation times in a variety of biological systems: lipid probe rotation in membranes,[23] internal motions of DNA,[24,25] acetylcholine receptor rotation in cell membrane,[10,26] rotation of antibodies and lipids associated with phospholipid monolayers,[11] and internal dynamics of chromatin in intact nuclei.[27] Detailed theory of PFPR has been described previously.[10,11,23,28–30] In these previous applications of PFPR the sample had a uniform orientation about the optical axis. In contrast, the labeled muscle fibers in the present study are an oriented sample. We give a brief description of the PFPR technique, followed by considerations for oriented samples.

PFPR is used to measure the rotational correlation time of molecules or small particles labeled with a fluorescent probe. This is accomplished by using a brief intense flash of polarized light to photobleach preferentially fluorescent probes whose absorption dipoles are parallel to the bleaching beam's polarization. Relaxation of the resulting anisotropic distribution of bleached fluorophore is measured by monitoring the postbleach fluorescence excited by a constant low-intensity polarized illumination. Two types of experiments are used, with the photobleach polarization parallel and perpendicular to the illumination polarization, yielding postbleach fluorescences $F_{\parallel}(t)$ and $F_{\perp}(t)$. An emission polarizer is oriented parallel to the illumination polarization.

Figure 1 shows PFPR results for rhodamine-labeled myosin subfragment 1 (R-S1) in 70% glycerol at −30°C and a photobleaching duration of 5 μs. For the parallel photobleach, the fluorophores whose absorption dipoles are aligned with the illumination polarization are preferentially photobleached. Thus the initial postbleach fluorescence for the parallel photobleach is deeper than for the perpendicular photobleach, which preferentially pho-

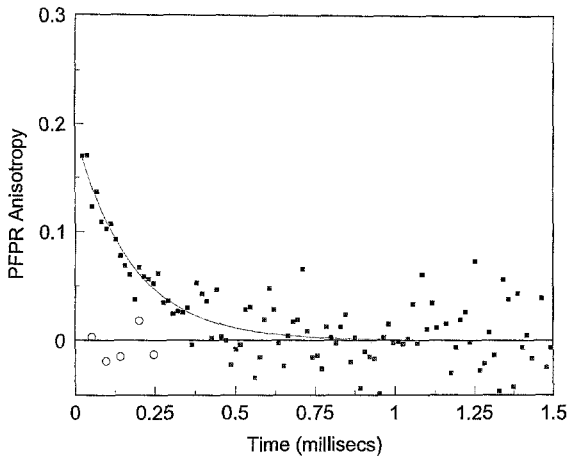

Fig. 2. PFPR anisotropy constructed from the data in Fig. 1 (filled squares) along with the best fit of Eq. (2), giving a rotational correlation time of 180 μs. PFPR anisotropy for R-S1 in 50% glycerol at $T = -10°C$ (open circles).

tobleaches those fluorophores whose absorption dipoles are perpendicular to the illumination polarization. As time goes on, the orientation distribution of photobleached fluorophore becomes uniform due to protein rotation. This causes the fluorescence intensity in the two types of photobleaching runs to become the same, as shown in Fig. 1. The rate at which the two fluorescence intensities join is a direct measure of the rotational correlation time of the protein.

The postbleach fluorescences $F_{\|}(t)$ and $F_{\perp}(t)$ are combined with the prebleach fluorescence F_{-} to form the PFPR anisotropy

$$r(t) = [\Delta F_{\|}(t) - \Delta F_{\perp}(t)] / [\Delta F_{\|}(t) + 2\Delta F_{\perp}(t)] \quad (1)$$

where $\Delta F_{\|,\perp}(t) = F_{-} - F_{\|,\perp}(t)$. The PFPR anisotropy decays to zero as the orientational distribution of bleached fluorophore becomes uniform. This behavior is analogous to the decay of a standard emission anisotropy (fluorescence or phosphorescence) due to rotation. Note, however, that the PFPR anisotropy defined in Eq. (1) is constructed from a "pump-and-probe" technique and is therefore different from the usual emission anisotropy, which is constructed from a "pump-only" technique. A detailed comparison of the PFPR anisotropy with other polarization techniques is given by Velez and Axelrod.[10] A notable difference is that the maximal possible value for the PFPR anisotropy for an isotropic immobile sample is 4/7, compared to 2/5 for a standard emission anisotropy.

For free tumbling in three dimensions Velez and Axelrod[10] show that the PFPR anisotropy decay can be approximated by

$$r(t) = A\exp(-6D_r t) \quad (2)$$

where D_r is the rotational diffusion coefficient and A is related to the depth of the photobleach, the amount of wobbling of the fluorophore during the bleach, and the angle between the fluorophore's absorption and its emission dipoles. Figure 2 shows the PFPR anisotropy constructed from the PFPR data curves in Fig. 1. Also shown is the best fit to Eq. (2), with a resulting rotational correlation time $1/6D_r$ of 180 μs.

We do not seek a general solution for $r(t)$ for an oriented sample with restricted motion. The rate of protein rotation is obtained simply from the rate of decay of $r(t)$. Orientation of the sample affects the size of the decrease in r with time, not the rate of the decrease. However, we are interested in the time zero PFPR anisotropy $r(0)$ for an oriented sample because $r(0)$ depends on how much rotation occurred during the photobleach pulse. $r(0)$ is obtained from Eq. (1) using the two fluorescences immediately after the photobleach, $F_{\|}(t = 0)$ and $F_{\perp}(t = 0)$. These time zero fluorescences are calculated by integration of an excitation term, a polarized emission term, and the initial postbleach distribution of unbleached fluorophore, $C_0(\Omega)$, over all orientations,

$$F(0) = \int d\Omega |\boldsymbol{\mu}\cdot\mathbf{e}_{excite}|^2 |\boldsymbol{\mu}\cdot\mathbf{e}_{emit}|^2 C_0(\Omega) \quad (3)$$

For the PFPR analysis we assume that the emission and absorption dipoles are parallel and designated by unit vector $\boldsymbol{\mu}$. (For rhodamine the angle between these dipoles is actually 15 to 20°, however, we let the effects of this nonzero angle be accounted for in the calculation of the wobble angle of the dipole described below.) For nonsaturating photobleaching pulses $C_0(\Omega)$ is the prebleach distribution $N(\Omega)$ times a first-order photobleaching term,

$$C_0(\Omega) = N(\Omega)\exp(-kt_{bl}|\boldsymbol{\mu}\cdot\mathbf{e}_{bleach}|^2) \quad (4)$$

where t_{bl} is the duration of the bleach pulse and k is the first-order rate constant for photobleaching. Saturating photobleaching pulses are considered in the Appendix.

The orientational distribution $N(\Omega)$ for an oriented sample such as rhodamine-labeled myosin heads in muscle fibers is expected to be cylindrically symmetrical about the fiber axis. Thus the distribution is $N(\theta)$, where θ is the polar angle measured from the fiber axis taking on values from 0 to 90°. Velez and Axelrod[10] showed that to get agreement between PFPR theory and experiment, it is necessary to allow for wobbling of the fluorophore's dipole during the photobleach pulse. This wobbling can be a combined effect of probe motion with respect to the protein and protein rotation that occurs during the bleach pulse. Wobbling is modeled by allow-

ing the absorption dipole to move within a cone of half-angle β during the bleach. In addition, we showed that saturation of the fluorophore's excitation transition during the bleach pulse also causes $r(0)$ to decrease.[31] This effect is treated in the Appendix.

Now we calculate the time zero postbleach fluorescences for bleach polarizations parallel and perpendicular to the illumination polarization for a muscle fiber which is oriented perpendicularly to the optical axis. Figure 3 shows two orientations of the illumination and bleach polarizations relative to the fiber. For an illumination polarization parallel to the fiber axis and with the emission polarizer parallel to the illumination polarization, the azimuthal integration about the fiber axis in Eq. (3) can be done, giving

$$F_{\parallel}(0) = 2\pi\int_0^{\pi/2} d\theta \sin\theta\cos^4\theta N(\theta) \exp\left[-kt_{bl}(A\cos^2\theta + B\sin^2\theta)\right] \quad (5)$$

$$F_{\perp}(0) = 2\pi\exp(-kt_{bl}B)\int_0^{\pi/2} d\theta \sin\theta\cos^4\theta N(\theta) \exp(-\alpha C) I_0(\alpha C) \quad (6)$$

and for an illumination polarization perpendicular to the fiber axis,

$$F_{\parallel}(0) = \pi\exp(-kt_{bl}B)\int_0^{\pi/2} d\theta \sin^5\theta N(\theta) \exp(-\alpha C)\left[\tfrac{3}{4}I_0(\alpha C) - I_1(\alpha C) + \tfrac{1}{4}I_2(\alpha C)\right] \quad (7)$$

$$F_{\perp}(0) = \tfrac{3}{4}\pi\int_0^{\pi/2} d\theta \sin^5\theta N(\theta) \exp\left[-kt_{bl}(A\cos^2\theta + B\sin^2\theta)\right] \quad (8)$$

where $\alpha = (kt_{bl}/2)\sin^2\theta$, I_i are modified bessel functions, and the wobble terms are

$$A = \frac{1-\cos^3\beta}{3(1-\cos\beta)} \quad (9)$$

$$B = \frac{\frac{2}{3} - \cos\beta + \frac{1}{3}\cos^3\beta}{2(1-\cos\beta)} \quad (10)$$

and $C = A - B$. Note that for no wobble $\beta = 0$, then $A = 1$ and $B = 0$.

A goal in our analysis is to determine the wobble angle β because this indicates the range of rotation of the protein during the bleaching pulse. Wobble angle β is determined by optimizing β in Eqs. (5)–(10) such that the resulting $r(0)$ created from Eq. (1) agrees with the measured value. Necessary quantities for this evaluation are the orientation distribution $N(\theta)$ and the bleach depth. We use steady-state fluorescence polarization measurements to determine a simple model for $N(\theta)$. The bleach depth is measured from the PFPR curves.

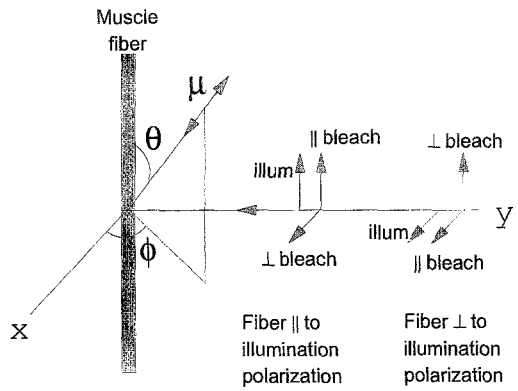

Fig. 3. Relative orientations of illumination and photobleaching polarizations with respect to muscle fiber. The laser beam is incident along the $-y$ direction. The fiber axis is perpendicular to the xy plane.

Determination of Orientational Distribution

Steady-state fluorescence polarization measurements made on muscle fibers are used to determine a model for the orientation distribution of the rhodamine-labeled myosin heads. Four fluorescence measurements, $F_{\parallel,\parallel}$, $F_{\parallel,\perp}$, $F_{\perp,\parallel}$, and $F_{\perp,\perp}$, are made from a fiber, where the first (second) subscript designates the polarization of the excitation (emission) polarizer with respect to the fiber axis. The absolute intensity is not used, thus these four fluorescences provide three ratios, from which three independent polarizations can be formed.[32]

$$P_{\parallel} = (F_{\parallel,\parallel} - F_{\parallel,\perp})/(F_{\parallel,\parallel} + F_{\parallel,\perp}) \quad (11)$$

$$P_{\perp} = (F_{\perp,\perp} - F_{\perp,\parallel})/(F_{\perp,\perp} + F_{\perp,\parallel}) \quad (12)$$

$$Q_{\parallel} = (F_{\parallel,\parallel} - F_{\perp,\parallel})/(F_{\parallel,\parallel} + F_{\perp,\parallel}) \quad (13)$$

Other sets of three independent polarizations could be defined but no advantage can be gained since all such sets come from the same three measured fluorescence ratios. We use a microscope for our measurements. In this configuration the excitation and emission optical paths are parallel. This is in contrast to the geometry in an L-format fluorescence spectrophotometer. Of the four fluorescences used in Eqs. (11)–(13), only $F_{\perp,\perp}$ is different in these two configurations. Therefore we use the notation $P_{\perp}^{L}$ and $F_{\perp,\perp}^{L}$ for the additional polarization and

fluorescence provided by the L-format, where

$$P^{L}_{\perp} = (F^{L}_{\perp,\perp} - F_{\perp,\parallel})/(F^{L}_{\perp,\perp} + F_{\perp,\parallel}) \quad (14)$$

We use a Gaussian model for the orientational distribution of the rhodamine dipoles of a labeled fiber.

$$N(\theta) = \frac{\exp\{-(\theta-\theta_0)^2/(2\theta_w^2)\}}{\theta_w(2\pi)^{\frac{1}{2}}} \quad (15)$$

The model is characterized by the peak of the distribution θ_o and the width θ_w. The distribution is valid from 0 to $\pi/2$ for the polar angle θ measured from the fiber axis.

If the absorption and emission dipoles are parallel, then $F_{\parallel,\perp} = F_{\perp,\parallel}$, so there are only two independent fluorescence ratio measurements and two independent polarizations from the microscope apparatus. In this case the three independent polarizations $P_{\parallel}$, $P_{\perp}$, and $P^{L}_{\perp}$ are used to determine the model's two parameters θ_o and θ_w. The steady-state fluorescences are

$$F_{\parallel,\parallel} = \int_0^{\pi/2} d\theta \sin\theta N(\theta) 2\cos^4\theta \quad (16)$$

$$F_{\parallel,\perp} = F_{\perp,\parallel} = \int_0^{\pi/2} d\theta \sin\theta N(\theta) \sin^2\theta\cos^2\theta \quad (17)$$

$$F_{\perp,\perp} = \int_0^{\pi/2} d\theta \sin\theta N(\theta) \tfrac{3}{4}\sin^4\theta \quad (18)$$

$$F^{L}_{\perp,\perp} = \frac{1}{3}F_{\perp,\perp} \quad (19)$$

The optimal values for θ_o and θ_w are found by varying θ_o and θ_w until the resulting polarizations $P_{\parallel}$, $P_{\perp}$, and $P^{L}_{\perp}$ calculated from Eqs. (11)–(14) and (16)–(19) have the best possible agreement with the measured values.

For comparison purposes we also use a model in which the absorption and emission dipoles are not parallel since as previously mentioned they are not quite parallel for rhodamine. In this model the emission dipole is equally likely to be oriented anywhere on a cone of half-angle ω about the absorption dipole, where ω is the angle between the absorption and the emission dipoles. $N(\theta)$ describes the distribution of the absorption dipoles. Then the equations for the fluorescences are

$$F_{\parallel,\parallel} = \int_0^{\pi/2} d\theta \sin\theta N(\theta) \{2\cos^2\omega\cos^4\theta + \sin^2\omega\cos^2\theta\sin^2\theta\} \quad (20)$$

$$F_{\parallel,\perp} = \int_0^{\pi/2} d\theta \sin\theta N(\theta) \{\cos^2\omega\sin^2\theta\cos^2\theta + \sin^2\omega\cos^2\theta(1-\tfrac{1}{2}\sin^2\theta)\} \quad (21)$$

$$F_{\perp,\parallel} = \int_0^{\pi/2} d\theta \sin\theta N(\theta) \{\cos^2\omega\sin^2\theta\cos^2\theta + \tfrac{1}{2}\sin^2\omega\sin^4\theta\} \quad (22)$$

$$F_{\perp,\perp} = \int_0^{\pi/2} d\theta \sin\theta N(\theta) \{\tfrac{3}{4}\cos^2\omega\sin^4\theta + \tfrac{1}{2}\sin^2\omega\sin^2\theta(1-\tfrac{3}{4}\sin^2\theta)\} \quad (23)$$

$$F^{L}_{\perp,\perp} = \int_0^{\pi/2} d\theta \sin\theta N(\theta) \{\tfrac{1}{4}\cos^2\omega\sin^4\theta + \tfrac{1}{2}\sin^2\omega\sin^2\theta(1-\tfrac{1}{4}\sin^2\theta)\} \quad (24)$$

These are used to calculate polarizations $P_{\parallel}$, $P_{\perp}$, $Q_{\parallel}$, and $P^{L}_{\perp}$, which are compared with the experimental values to determine the distribution $N(\theta)$ as described above. The angle ω either can be left as a free parameter to be determined along with θ_o and θ_w or can be given a previously determined value.

MATERIALS AND METHODS

Preparation of Rhodamine-Labeled Fibers

Solutions used were as follows. Rigor solution is 80 m*M* KCl, 5 m*M* potassium phosphate, pH 7, 5 m*M* $MgCl_2$, 2 m*M* EGTA, and 1 m*M* dithiothreitol (DTT). ADP solution is rigor plus 4 m*M* ADP. Relaxing solution is rigor plus 4 m*M* ATP. Active solution is rigor minus EGTA, plus 4 m*M* ATP and 0.1 m*M* $CaCl_2$. Active solutions containing an ATP regenerating system consisting of 4 m*M* phosphocreatine and 0.4 mg/ml creatine kinase were also used to confirm that ATP was not significantly depleted during data collection.

Rabbit psoas muscle fibers were obtained and stored in relaxing solution containing 50% glycerol (v/v) at −15°C for up to several weeks.[12] The skinned fibers were labeled with 70 μ*M* 5'-(iodoacteamido) tetramethylrhodamine (5'-IATR; Molecular Probes, Eugene,

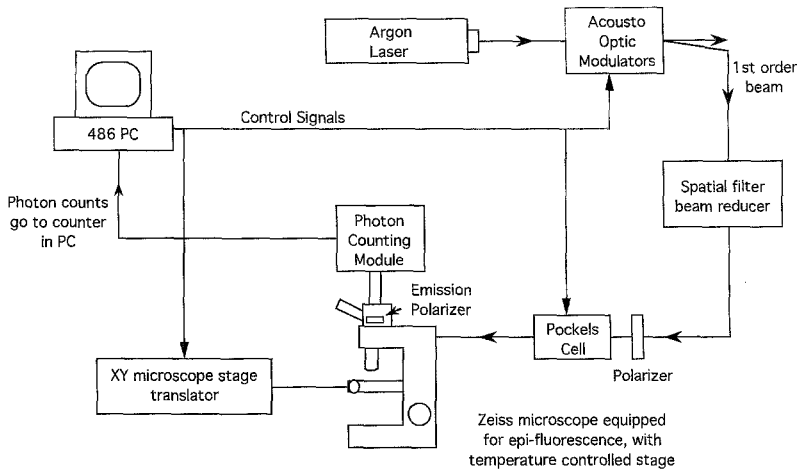

Fig. 4. Apparatus for PFPR experiments.

OR) in relaxing solution without DTT and the excess dye was washed out with relaxing solution.[19,33]

Labeled fibers were placed in the desired solution between fused silica slides and placed on the microscope stage at 6°C. For active fibers we rinsed first with relaxing solution without EGTA before adding active solution. For active fibers the ends of the fiber were superglued to the fused silica slide. PFPR data collection for active fibers was completed in less than 10 min from the time the fiber was exposed to active solution. Fluorescence polarization measurements were made before and after PFPR data collection as a check on fiber integrity.

Preparation and Labeling of Myosin Subfragment 1

Rabbit myosin was prepared by a standard method.[34] S1 was prepared by digesting myosin filaments with α-chymotrypsin.[35] The 5'-IATR treatment of S1 was performed in a 1.2 molar excess of dye to protein in 50 m*M* TES buffer at pH 7 and 4°C for 12 h. The reaction was stopped by separating the labeled proteins from the dye on a Sephadex G 25 column equilibrated with 50 m*M* TES at pH 7. The protein was then dialyzed in rigor buffer in the presence of 0.1 m*M* PMSF. The labeled S1 contained 0.45–0.70 mol tetramethylrhodamine/mol of S1.

Preparation of Immobilized Rhodamine

Rhodamine B was dissolved in ethanol at about 1 mg/ml. Drops of the dissolved fluorophore were mixed into silicone vacuum grease (Dow Corning high-vacuum grease) until the grease was slightly colored, nominally 20 μ*M*. A layer of the grease < 1 mm was placed between fused silica slides.

Polarized Fluorescence Photobleaching Recovery Apparatus

Figure 4 shows the optical setup. The 514-nm line of an argon ion laser (Coherent Innova 90) was used for fluorescence excitation and photobleaching. Two acoustooptic modulators (IntraAction ME-40) in series were used to control the laser beam intensity. After the modulators the beam passed through a spatial filter (25-μm)/beam diameter reducer, then through a Pockels Cell (Lasermetrics EOM-3079) to control polarization. Epiillumination on an upright microscope (Zeiss Axioplan) equipped with a 20×, 0.5 NA, Zeiss Plan-Neofluar air objective lens was used to focus the laser beam onto the sample. Fluorescence collected by the objective lens passed through the dichroic mirror, a barrier filter, an emission polarizer oriented parallel to the illumination polarization, an image plane diaphragm, and a lens which focused the fluorescence onto the active area of a photodiode detector module (EG&G Optoelectronics SPCM-200-PQ). Laser beam power output was 600 mW. Due to losses in the optical path, the maximum laser beam power at the sample plane of the microscope stage was 200 mW, which occurred during the photobleaching pulse. The low-level laser illumination intensity was approximately 20 μW. In all experiments the background fluorescence was negligible compared to the rhodamine emission.

Intensities of the parallel and perpendicular bleaching polarizations were checked by passing the laser illumination through the sample plane and through neutral

density filters onto a photodiode. The two intensities were equalized by independently setting their control voltages sent to the acoustooptic modulator driver.

The sample was placed on an automated *xy*-translating stage (Ludl Electronics Products Ltd.) mounted on the microscope. Cooling of the sample on the stage was accomplished by use of a Peltier junction device (Physitemp) and by blowing evaporated nitrogen supplied by a Bruker variable-temperature unit (ER 4111 VT).

The PFPR experiment was controlled by a 486 PC and a custom-written Fortran and assembly language program (a modified version of a program generously provided by Dan Axelrod, University of Michigan, Ann Arbor). Photon counts from the photodiode detector module were counted by a counter/timer board (Keithley MetraByte CTM-05) in the PC. Photobleaching durations which gave good bleach depths were 5 μs for the R-S1 in 70% glycerol control experiments and 200 μs in muscle fiber experiments. This difference is due to the environmental sensitivity of the photobleachability of a fluorophore. Sample times were 15 μs for R-S1 in glycerol/aqueous buffer, 300 μs for muscle fibers in rigor and ADP, 300 μs for relaxed fibers aligned parallel to the illumination polarization, 2.5 ms for relax aligned perpendicularly, and 2.5 ms for fibers in isometric contraction.

Sample heating was estimated by the method outlined previously.[10] We obtained a steady-state temperature rise of 10°C during the bleaching pulse, for the ~50 μ*M* myosin in muscle fibers and a typical labeling ratio of 0.4 probe per myosin head. There was no temperature gradient from the observation illumination. Temperature rise from, and relaxation to, the bathing solution temperature (6°C) was instantaneous on the time scale of our experiments so that there was a significant temperature gradient only during the bleaching pulse. The bleach pulse temperature gradient was confined to the illuminated region of ~10 μm². Muscle fiber function is not harmed by this mild and very localized heating.

For a typical experiment $F_{\parallel}(t = 0) = (1/2)F_{-}$, $F_{\perp}(t = 0) = (^2/_3)F_{-}$, and, from Eq. (1), the uncertainty in the anisotropy goes as $\sqrt{1/F_{-}}$ in photon counts per sample time. Therefore getting a good signal-to-noise ratio with count rates of tens of thousands of counts per second and a 300-μs sample time required signal averaging of around a thousand runs. For the 2.5-ms sample time a couple hundred runs were signal averaged.

The Pockels cell is driven by a custom-built amplifier so that nominally 0 V at the Pockels Cell provides the illumination polarization.

Another custom-written Fortran and assembly language program uses the PFPR apparatus to measure the fluorescence polarizations $P_{\parallel}$, $P_{\perp}$, and $Q_{\parallel}$ for rhodamine-labeled fibers.

Data Analysis

The orientation distribution of the rhodamine dipoles on fibers was determined by minimizing the difference between the measured polarizations and those calculated from Eqs. (11)–(14) as described in the previous section. The minimum was found by performing a two-dimensional grid search over the peak and width of the Gaussian distribution. The angle between absorption and emission dipoles was set to 17° determined from the steady-state fluorescence polarization of 0.44 for isotropic rhodamine. However, the resulting distribution did not depend strongly on this angle.

The wobble angle β, which indicates the range of rotation of the probe during the bleach pulse, was determined by varying β and a bleach depth parameter as described under Theory so that the calculated time zero anisotropy and bleach depth agreed with the experimental values. The experimental values of $r(0)$ were either read directly from the data or determined by extrapolation if reversible bleaching occurred (which is discussed later). Extrapolation was trivial since the anisotropies were constant after any reversible bleaching recovery except for the anomalous behavior of the ADP fiber oriented perpendicularly to the illumination polarization, which is discussed later. Others have observed reversible photobleaching in PFPR experiments and discussed its origin.[10,25,27]

In the Appendix we show that saturation during the bleach pulse needed to be taken into account. Therefore during the determination of the wobble angle β, the bleach parameter that was varied was k_b (defined in the Appendix), not the first-order parameter k used in Eq. (4), to match the experimental bleach depth.

RESULTS

Figures 1, 2, and 5 show results from control experiments demonstrating that the PFPR apparatus works properly. Figure 1 shows results from a PFPR experiment performed on a sample of R-S1 in 70% glycerol at $T = -30$°C, which is predicted to have a rotational correlation time much longer than the 5-μs photobleaching duration. As predicted for slow free tumbling, the two recovery curves merge to the same value. Figure 2 shows the PFPR anisotropy $r(t)$ formed from the two recovery curves in Fig. 1 using Eq. (1). Also shown is the best fit using Eq. (2), yielding a rotational correlation

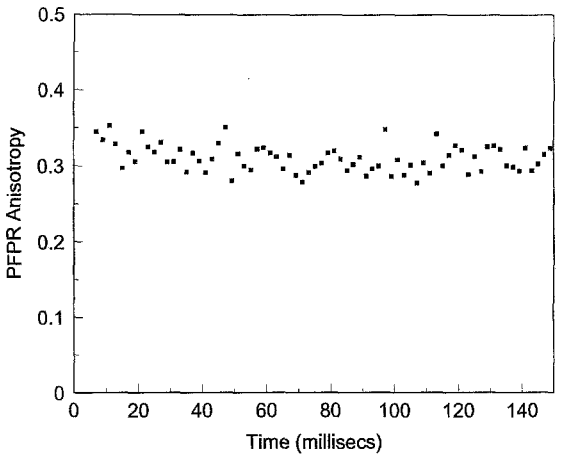

Fig. 5. PFPR anisotropy for rhodamine B immobilized in silicone vacuum grease.

time of 180 μs. Figure 2 also shows the resulting PFPR anisotropy for R-S1 in 50% glycerol at $T = -10°C$. In this case the rotational correlation time is predicted to be less than the photobleach duration, thus allowing the fluorophore to rotate significantly during the photobleaching pulse, resulting in orientation independent photobleaching. The two fluorescence recovery curves were identical, resulting in a constant value of zero for the PFPR anisotropy shown in Fig. 2. Figure 5 shows that the PFPR anisotropy for rhodamine B immobilized in silicone vacuum grease is nonzero and constant.

Figure 6 shows PFPR anisotropies for rhodamine-labeled glycerinated muscle fibers oriented parallel and perpendicularly to the illumination polarization for the four states of rigor, ADP, relax, and active isometric contraction at $T = 6°C$ using a 200-μs photobleaching pulse. None of the cases show a substantial decay of anisotropy from which a rotational correlation time can be deduced. Instead the constant values of the anisotropies are used to estimate wobble angles which describe the range of rotation of the labeled protein during the photobleaching pulse. In rigor and ADP the anisotropies are constant and relatively large compared to relax and active. Possible causes of the anomalous rise of $r(t)$ at early times for rigor and the noisy results for ADP fibers oriented perpendicularly to the illumination polarization are discussed in the next section.

Table I shows the measured steady-state fluorescence polarizations $P_{\|}$, $P_{\perp}$, and $Q_{\|}$ for the fibers in the various states. Also shown are measured values for $P_{\perp}^{L}$ from Ajtai *et al.*[18] Gaussian distributions for the labeled myosin heads were determined by varying the peak θ_0 and width θ_w in Eq. (15) so that the calculated polarizations from Eqs. (11)–(14) and (16)–(24) gave the best possible agreement with the measured values. The best-fit parameters for the peak and width of the Gaussian distributions are shown in Table II and their corresponding calculated steady-state fluorescence polarizations are shown in Table I for comparison with the measured values. In these calculations the angle between absorption and emission dipoles was set at 17°, which was deduced from the measured value of 0.43 for the steady-state fluorescence polarization for R-S1 in 70% glycerol. However, making the assumption that the dipoles are parallel results in only slightly different Gaussian distributions and no difference in wobble angles calculated using these distributions.

The wobble angles were calculated by varying β in Eqs. (9) and (10) so that the calculated PFPR anisotropies and bleach depths matched the measured values. The best-fit wobble angles are shown in Table II. For comparison, this procedure finds that the wobble angle is 30° for immobilized rhodamine and 90° for rapid freely tumbling rhodamine. In these calculations we included the effects of saturation of the fluorophore's excitation transition during the photobleaching pulse as described in the Appendix.

DISCUSSION

PFPR Technique

The PFPR technique is relatively new and unknown, therefore before addressing the muscle fiber results, we first point out that the control experiments demonstrate the validity of the PFPR technique. The PFPR anisotropy in Fig. 2 constructed from the PFPR data in Fig. 1 for R-S1 in solution shows the expected decay to zero for protein tumbling slowly compared to the 5-μs photobleach duration. The rotational correlation time of 180 μs is about 1000 times slower than that of S1 in aqueous buffer.[36] This agrees with the predicted effect of viscosity since the viscosity of 70% glycerol at −30°C is approximately 1000 times that of water at room temperature. Figure 2 also shows that when the viscosity was lowered, thus allowing R-S1 to rotate significantly during the photobleaching pulse, the PFPR anisotropy was zero. For immobilized rhodamine Fig. 5 shows that the PFPR anisotropy is constant and nonzero.

The results of these control experiments are all as expected for properly functioning PFPR apparatus. They demonstrate that PFPR can measure a rotational correlation time for samples rotating slowly compared to the photobleaching duration and that, for samples which ro-

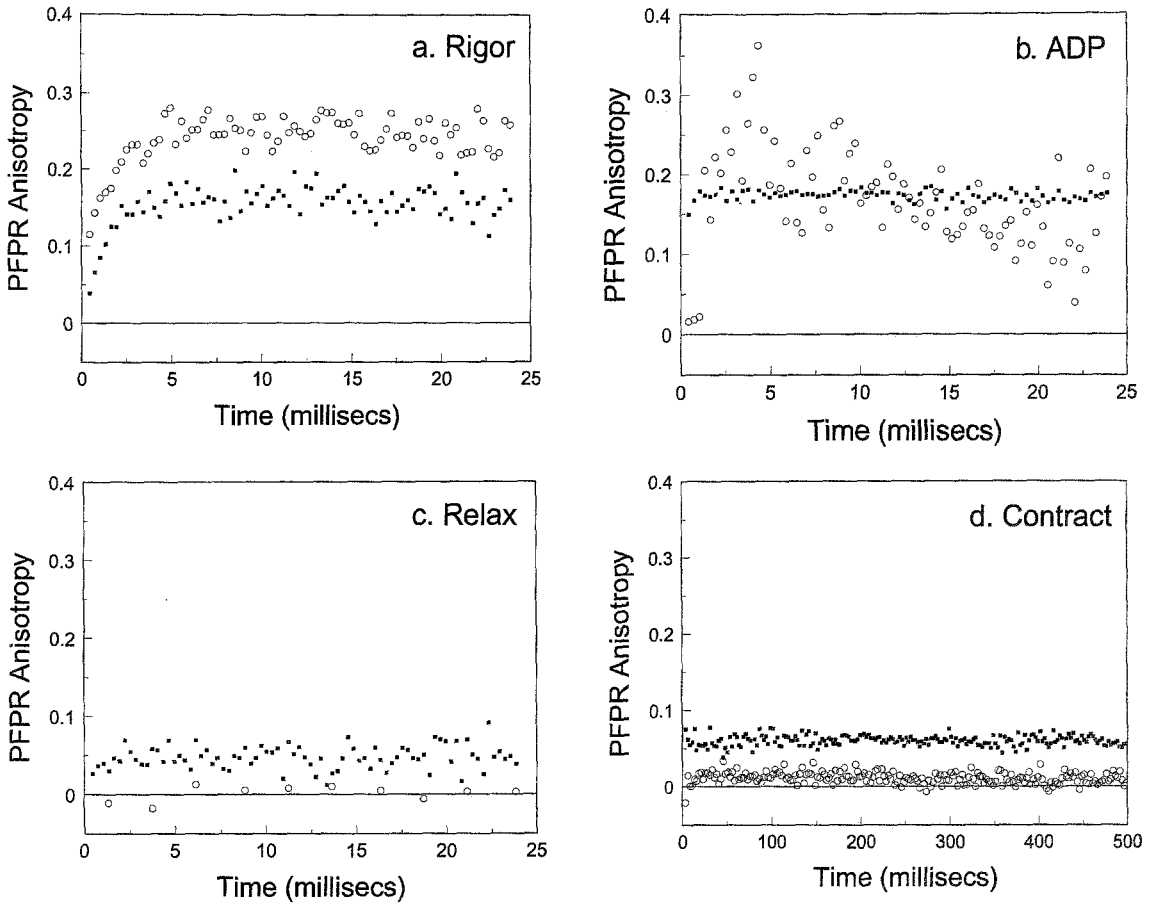

Fig. 6. PFPR anisotropies for muscle fibers oriented parallel and perpendicularly to the illumination polarization for each of the four states: (a) rigor; (b) ADP; (c) relax; (d) isometric contraction. The photobleaching duration was 0.2 ms. Open circles and filled squares are for fibers aligned perpendicularly and parallel to the illumination polarization, respectively.

Table I. Comparison of Measured Fluorescence Polarizations (±0.03) with Those Calculated Using Best-Fit Gaussian Orientational Distributions for Rhodamine-Labeled Fibers

	$P_\parallel$	$P_\perp$	$Q_\parallel$	$P_\perp{}^L$
Rigor				
Measured	0.25	0.61	0.24	0.20[a]
Calculated	0.25	0.55	0.20	0.14
ADP				
Measured	0.61	0.14	0.58	−0.23[a]
Calculated	0.57	0.18	0.62	−0.28
Relax				
Measured	0.43	0.37	0.41	−0.02[a]
Calculated	0.42	0.40	0.43	−0.05
Active				
Measured	0.50	0.30	0.50	−0.13[a]
Calculated	0.49	0.31	0.52	−0.15

[a]Measured value from Ajtai *et al.* [18].

Table II. Best-Fit Gaussian Orientational Distributions and Best-Fit Wobble Angle Parameters for Rhodamine-Labeled Fibers

	Gaussian parameters (θ_o, θ_w)	Wobble angle ($\beta \pm 5°$)
Rigor	90, 41	44°
ADP	0, 41	55°
Relax	48, 44	82°
Active	24, 44	78°

tate significantly during the photobleaching pulse, PFPR can provide an upper bound for the rotational correlation time. Therefore the usefulness of PFPR is not limited to times longer than the photobleaching duration. The demonstrated capabilities of PFPR make it a potentially use-

ful technique, new to muscle research, well suited to the investigation of partially restricted motions which are likely for myosin heads in muscle fibers.

Fiber Results

Here we discuss the results of this first application of PFPR to muscle fibers, along with some of the problems which arose. The PFPR results for the fibers give information about the rate and range of rotation of the myosin heads. In all cases, except possibly ADP oriented perpendicularly to the illumination polarization, the PFPR anisotropy does not decay. Therefore any rotation which occurs is faster than the millisecond time resolution of our experiment. The range of fast rotation is deduced from the magnitudes of the time zero PFPR anisotropies which are either read directly or extrapolated from the graphs in Fig. 6. The fact that the PFPR anisotropies are higher in rigor and ADP than in relax and active indicates that the range of this fast motion is much smaller in rigor and ADP. The range of the fast rotation is quantified by the wobble angles in Table II, which can be compared with the wobble angles of 30° for immobile rhodamine and 90° for freely tumbling rhodamine. Thus myosin heads are close to immobile in rigor, slightly more mobile in ADP, substantially more mobile in active isometric contraction, and the most mobile in relax.

The orientation distributions in Table II show that the orientation of the myosin heads in fibers is strongly dependent on the physiological state of the fiber. The ratio of the distribution's maximum value to its minimum value is 10 for rigor and ADP, slightly less than 2 for relax, and slightly more than 2 for active isometric contraction, thus demonstrating that the distributions for rigor and ADP are more highly oriented than for relax and active isometric contraction. The distribution for relax is the closest to uniform and that for active isometric contraction is between those for ADP and relax. The peak of the Gaussian distribution changes from perpendicular to the fiber axis for rigor to parallel to the fiber axis for ADP. However the average polar angle from the fiber axis calculated using the Gaussian distributions and the $\sin\theta$ solid angle factor changes from 65° for rigor to 44° for ADP.

Andreev *et al.*[17] found that for decorated fibers in rigor, the orientational distribution of the myosin heads is different for partial versus full decoration. This suggests that a single Gaussian may not be adequate for modeling the distribution. However, for our purpose of obtaining a distribution function for use in Eqs. (5)–(8), the difference between the two distributions shown in Fig. 8 of Andreev *et al.*[17] is small enough so that a single Gaussian can be used.

The PFPR anisotropy curves for both orientations of the rigor fiber and the ADP perpendicular orientation have some anomalous behavior. The two curves for rigor show increasing anisotropy for the first couple of msecs. This type of behavior has been seen before in PFPR[10] and in the related technique of fluorescence depletion anisotropy.[37] Velez and Axelrod[10] show that if the sample is heterogeneous, then the effect of reversible photobleaching does not cancel out in the construction of the PFPR anisotropy, $r(t)$, in Eq. (1). This can lead to anomalous behavior of $r(t)$ during the reversible photobleaching recovery time. Interestingly, the reversible photobleaching recovery time depended on the physiological state of the muscle fiber. For muscle fibers in rigor the recovery was complete in 2 ms and for ADP and relax the time was 1 ms. For contraction reversible photobleaching was not detected, probably because a 2.5-ms sample time was used for this state, compared to the 0.3-ms sample time used for the other states. It appears that the longer reversible photobleaching recovery times are correlated with increasingly restricted motion. The net effect for these fiber studies is that the time resolution was millisecond instead of the 0.2-ms determined by the photobleaching duration.

For the ADP fiber oriented perpendicularly to the illumination polarization, Table II shows that the myosin heads are attached to actin so that the dipoles tend toward being perpendicular to the illumination polarization. In addition to causing a low fluorescence signal, we think that this may be related to the anomalous behavior for $r(t)$ in Fig. 6b. For this case the postbleach fluorescence for the perpendicular bleach had an initial rapid increase (due to reversible photobleaching recovery) followed by a slow decay to its final value. This caused the peak and slow decay apparent in Fig. 6b. This is the only case where such a peak occurred. We speculate that this peak is due to the bleach pulse causing some myosin heads to become detached from actin, allowing them to be able to rotate their dipoles closer to parallel to the illumination polarization, thus causing an increase in fluorescence. The fluorescence then decreases as the heads reattach to actin, thus returning their dipole orientations toward perpendicular to the illumination polarization. Unresolved problems with this explanation are the lack of the specific mechanism responsible for the light-induced detachment of the rhodamine-labeled myosin heads from actin and that it requires unusually slow rebinding of the myosin heads to actin.

In our model the wobble angle parameter β indicates the range of wobbling that occurs during the pho-

tobleaching pulse. This parameter includes probe wobble with respect to the protein during the bleach, protein rotation during the bleach, nonzero angle between absorption and emission dipoles, and depolarizing effects due to a nonideal apparatus. Therefore a particular value for β does not have clear physical significance. However, the relative value of β compared to values for immobile and rapidly mobile samples are significant. Ajtai *et al.*[18] showed that probe wobble with respect to the protein is not affected by presence of nucleotide for the 5' isomer of IATR labeling SH1, therefore differences in β for fibers in the various states do reflect different amounts of rotation of the myosin head during the bleach pulse. We emphasize that β is not an actual angle of rotation but, instead, should be considered as a parameter used for relative comparison of the myosin head's range of motion in fibers in the various physiological states during the 200-μs bleaching pulse.

In our PFPR and wobble analysis we assumed that the absorption and emission dipoles are parallel. There is no benefit from the complicated modification of Eqs. (5)–(8) in order to include a nonzero angle between absorption and emission dipoles, since the resulting angle deduced from fluorescence polarization measurements is small and the calculated wobble angle is a parameter used only for relative comparisons. For our analysis the wobble angle includes the effect of a nonzero angle between the absorption and the emission dipoles. For example, part of the 30° wobble for immobile dye is due to the 17° angle between absorption and emission dipoles. But we make no conclusions based on the absolute magnitudes of the wobble angles, only on their relative values. Therefore our conclusions regarding rotation of the myosin head in the various physiological states and relative to immobile dye and completely free dye are not invalidated by the approximation that rhodamine's absorption and emission dipoles are parallel.

Comparison to Other Work

Our PFPR results are in good agreement with previous EPR[5–7] and phosphorescence[9] studies which investigated shorter time scales than this study and found that myosin heads in fibers have virtually no motion in rigor, considerable submillisecond motion in relax, and slightly less motion in contraction.

The orientation results, in general, agree with previous results from EPR[2,3,13,14] and fluorescence polarization.[4,17–21] However, the EPR methods[2,14] report a rigor to ADP rotation smaller than the 20° rotation of the average polar angle found here. These differences are reconciled with consideration of the relative probe to protein orientation in determining probe sensitivity to cross-bridge rotation.[1,2,22]

The PFPR results can be compared with the final values of the time-resolved fluorescence anisotropy decay results of Burghardt and Thompson.[38] Figure 2 in that work shows that the anisotropy for rigor has leveled off to a value of 0.32 at 150 ns and that for relax the anisotropy is 0.27 at 150 ns but is still decaying. Using their parameters for the two exponential fits to the anisotropies gives $r(t = \infty)$ values of 0.32 for rigor and 0.05 for relax. These results are compatible with our PFPR results of a relatively high PFPR anisotropy for rigor and a low one for relax.

Conclusion

We have presented the first time application of PFPR to muscle fibers, along with the first application of PFPR to an oriented system (one which is not cylindrically symmetric about the optical axis). In spite of some problems which we discussed, the overall success of this application of PFPR to muscle fibers is demonstrated by the good agreement of the PFPR results with published results from other spectroscopic techniques.

Improvement of this application of PFPR to muscle fibers may be possible by using a fluorescent probe which bleaches more easily and has less, or faster, reversible photobleaching than rhodamine, while retaining rhodamine's desirable S1 binding properties regarding tightness and specificity. In addition, Yuan and Axelrod[39] have recently shown that PFPR anisotropies greater than 0.2 can be obtained from 0.5-ns bleach pulses from N2/dye laser flashes on samples of rhodamine-labeled α-bungarotoxin. This advance means that the PFPR time scale can potentially go from a few nanoseconds to essentially infinite. However, practical applications of this submicrosecond PFPR have not yet been demonstrated.

The results of highly oriented and restricted myosin heads in the rigor and ADP states and nearly uniform and highly mobile heads in the relax state are consistent with a scheme in which myosin heads bind in different conformations to actin in the rigor and ADP states and bind transiently in the relax state. The results for the active isometric state give no evidence of a high-amplitude rotation of the cross-bridge on the time scale of milliseconds to seconds. Given that our other work has led us to believe that the cross-bridge rotates through a large angle (35–45°) during contraction,[1] and that the active cross-bridge rotation is expected to be slowest in the isometric contraction, our results suggest that the major cross-bridge rotational movement during contraction

occurs in the submillisecond time domain. We cannot, however, rule out the possibility that rather lower-amplitude millisecond or slower rotational motions occur which are obscured by the high-amplitude submillisecond rotations.

APPENDIX

Here we consider the effect of saturation of the fluorophore's transition from its ground state to its first excited electronic state during the photobleaching pulse. The first-order photobleaching term in Eq. (4) is good only if the excitation rate is much less than the deexcitation rate. If this is not the case, then Hellen and Burghardt[31] have shown that the appropriate photobleaching term is

$$\exp\{-k_b t_{bl}/[1 + k_f/(k_e|\boldsymbol{\mu}\cdot\mathbf{e}_{bleach}|^2)]\} \quad \text{(A1)}$$

where $k_e\,|\boldsymbol{\mu}\cdot\mathbf{e}_{bleach}|^2$ is the excitation rate for transitions from the ground state to the first excited electronic state, k_f is the deexcitation rate for transitions (radiative and nonradiative) from the first excited state to the ground state, and k_b is the rate of transitions from the excited state to the photobleached state. k_e is proportional to the incident intensity. Note that for photobleaching with a low-intensity excitation ($k_e \ll k_f$), this becomes the first-order photobleaching term used in Eq. (4), where

$$k = k_b k_e / k_f \quad \text{(A2)}$$

Now we estimate the ratio of the excitation rate to deexcitation rate, k_e/k_f. The rate of absorptions per second is

$$k_e = I \times \sigma \quad \text{(A3)}$$

where I is the number of photons per second per unit area for the bleaching beam and σ is the absorption cross section for the fluorophore. For a 200-mW, 514-nm photobleaching beam focused to 10 μm^2 and $\sigma = 1$ Å^2, one calculates that $I = 5 \times 10^{16}$ photons/(s $\times$ μm^2) and $k_e = 5 \times 10^8$ s^{-1}. A typical fluorescence lifetime is a few nanoseconds, which gives $k_f \sim 3 \times 10^8$ s^{-1}. So we estimate $k_e/k_f \approx 1.5$, which requires the use of Eq. (A1) for the photobleaching term.

The time zero PFPR fluorescences for illumination polarization parallel to the muscle fiber are now

$$F_{\parallel}(0) = 2\pi \int_0^{\pi/2} d\theta \sin\theta\cos^4\theta N(\theta) \exp\left[\frac{-k_b t_{bl}}{1 + (k_f/[k_e\,(A\cos^2\theta + B\sin^2\theta)])}\right] \quad \text{(A4)}$$

$$F_{\perp}(0) = \int_0^{2\pi} d\phi \int_0^{\pi/2} d\theta \sin\theta\cos^4\theta N(\theta) \exp\left[\frac{-k_b t_{bl}}{1 + (k_f/[k_e\,(B + C\sin^2\theta\sin^2\phi)])}\right] \quad \text{(A5)}$$

and those for illumination polarization perpendicular to the muscle fiber are

$$F_{\parallel}(0) = \int_0^{2\pi} d\phi \int_0^{\pi/2} d\theta \sin^5\theta\sin^4\phi N(\theta) \exp\left[\frac{-k_b t_{bl}}{1 + (k_f/[k_e\,(B + C\sin^2\theta\sin^2\phi)])}\right] \quad \text{(A6)}$$

$$F_{\perp}(0) = \tfrac{3}{4}\pi \int_0^{\pi/2} d\theta \sin^5\theta N(\theta) \exp\left[\frac{-k_b t_{bl}}{1 + (k_f/[k_e\,(A\cos^2\theta + B\sin^2\theta)])}\right] \quad \text{(A7)}$$

where A, B, and C were defined in Eqs. (9) and (10).

Wobble angles were determined as described in the text except that Eqs. (A4)–(A7) were used in place of Eqs. (5)–(8). k_e/k_f was set to 1.5, and the photobleach parameter $k_b t_{bl}$ was varied so that the calculated bleach depth matched the experimental value.

ACKNOWLEDGMENTS

We thank Daniel J. Toft for help with the labeling of the muscle fibers and Jacqueline Lafky for help in typing the manuscript. This work was supported by National Institutes of Health Grant R01 AR 39288, American Heart Association Grant-in-Aid 930 06610, and the Mayo Foundation.

REFERENCES

1. K. Ajtai, D. J. Toft, and T. P. Burghardt (1994) *Biochemistry* **33**, 5382–5391.
2. K. Ajtai, A. Ringler, and T. P. Burghardt (1992) *Biochemistry* **31**, 207–217.
3. K. Ajtai, A. R. French, and T. P. Burghardt (1989) *Biophys. J.* **56**, 535–541.
4. T. P. Burghardt, T. Ando, and J. Borejdo (1983) *Proc. Natl. Acad. Sci. USA* **80**, 7515–7519.

5. C. L. Berger and D. D. Thomas (1993) *Biochemistry* **32**, 3812–3821.
6. V. A. Barnett and D. D. Thomas (1989) *Biophys. J.* **56**, 517–523.
7. D. D. Thomas, S. Ishiwata, J. C. Seidel, and J. Gergely (1980) *Biophys. J.* **32**, 873–890.
8. D. W. Hayden, S. Ramachandran, and D. D. Thomas (1994) *Biophys. J.* **66**, A189.
9. R. A. Stein, R. D. Ludescher, P. S. Dahlberg, P. G. Fajer, R. L. H. Bennett, and D. D. Thomas (1990) *Biochemistry* **29**, 10023–10031.
10. M. Velez and D. Axelrod (1988) *Biophys. J.* **53**, 575–591.
11. M. M. Timbs and N. L. Thompson (1990) *Biophys. J.* **58**, 413–428.
12. J. Borejdo, S. Putnam, and M. F. Morales (1979) *Proc. Natl. Acad. Sci. USA* **76**, 6346–6350.
13. D. D. Thomas and R. Cooke (1980) *Biophys. J.* **32**, 891–906.
14. P. G. Fajer, E. A. Fajer, J. J. Matta, and D. D. Thomas (1990) *Biochemistry* **29**, 5865–5871.
15. P. G. Fajer (1994) *Proc. Natl. Acad. Sci. USA* **91**, 937–941.
16. C. L. Berger, J. S. Craik, D. R. Trentham, J. E. T. Corrie, and Y. E. Goldman (1994) *Biophys. J.* **66**, A234.
17. O. A. Andreev, A. L. Andreev, and J. Borejdo (1993) *Biophys. J.* **65**, 1027–1038.
18. K. Ajtai, P. J. K. Ilich, A. Ringler, S. S. Sedarous, D. J. Toft, and T. P. Burghardt (1992) *Biochemistry* **31**, 12431–12440.
19. K. Ajtai and T. P. Burghardt (1986) *Biochemistry* **25**, 6203–6207.
20. K. Ajtai and T. P. Burghardt (1987) *Biochemistry* **26**, 4517–4523.
21. J. Borejdo, O. Assulin, T. Ando, and S. Putnam (1982) *J. Mol. Biol.* **158**, 391–414.
22. T. P. Burghardt and K. Ajtai (1994) *Biochemistry* **33**, 5376–5381.
23. L. M. Smith, R. M. Weis, and H. M. McConnell (1981) *Biophys. J.* **36**, 73–91.
24. B. A. Scalettar, P. R. Selvin, D. Axelrod, J. E. Hearst, and M. P. Klein (1988) *Biophys. J.* **53**, 215–226.
25. B. A. Scalettar, P. R. Selvin, D. Axelrod, M. P. Klein, and J. E. Hearst (1990) *Biochemistry* **29**, 4790–4798.
26. M. Velez, K. F. Barald, and D. Axelrod (1990) *J. Cell Biol.* **110**, 2049–2059.
27. P. R. Selvin, B. A. Scalettar, J. P. Langmore, D. Axelrod, M. P. Klein, and J. E. Hearst (1990) *J. Mol. Biol.* **214**, 911–922.
28. W. A. Wegener and R. Rigler (1984) *Biophys. J.* **46**, 787–793.
29. W. A. Wegener (1984) *Biophys. J.* **46**, 795–803.
30. R. E. Dale (1987) *Eur. Biophys. J.* **14**, 179–193.
31. E. H. Hellen and T. P. Burghardt (1994) *Biophys. J.* **66**, 891–897.
32. W. G. A. Wilson and R. A. Mendelson (1983) *J. Muscle Res. Cell Motil.* **4**, 671–693.
33. J. Borejdo and S. Putnam (1977) *Biochim. Biophys. Acta* **459**, 578–595.
34. Y. Tonomura, P. Appel, and M. F. Morales (1966) *Biochemistry* **5**, 515–521.
35. A. G. Weeds and R. S. Taylor (1975) *Nature* **257**, 54–56.
36. R. A. Mendelson, M. F. Morales, and J. Botts (1973) *Biochemistry* **12**, 2250–2255.
37. T. M. Yoshida and B. G. Barisas (1986) *Biophys. J.* **50**, 41–53.
38. T. P. Burghardt and N. L. Thompson (1985) *Biochemistry* **24**, 3731–3735.
39. Y. Yuan and D. Axelrod (1994) *J. Fluoresc.* **4**, 141–151.